

TERRESTRIAL PHOTOGRAMMETRY VS LASER SCANNING FOR RAPID EARTHQUAKE DAMAGE ASSESSMENT

C. Vasilakos^{1,*}, S. Chatzistamatis², O. Roussou¹, N. Soulakellis¹

¹ Dept. of Geography, University of the Aegean, Mytilene, Greece - (chvas, orousou, nsoul)@aegean.gr

² Dept. of Cultural Technology and Communication, University of the Aegean, Mytilene, Greece - stami@aegean.gr

KEY WORDS: Terrestrial photogrammetry, Structure from Motion, Laser scanning, Earthquake damage assessment, Point clouds

ABSTRACT:

Building damage assessment caused by earthquakes is essential during the response phase following a catastrophic event. Modern techniques include terrestrial and aerial photogrammetry based on Structure from Motion algorithm and Laser Scanning with the latter to prove its superiority in accuracy assessment due to the high-density point clouds. However, standardized procedures during emergency surveys often could not be followed due to restrictions of outdoor operations because of debris or decrepit buildings, the high human presence of civil protection agencies, expedited deployment of survey team and cost of operations. The aim of this paper is to evaluate whether terrestrial photogrammetry based on a handheld amateur DSLR camera can be used to map building damages, structural deformations and facade production in an accepted accuracy comparing to laser scanning technique. The study area is the Vrisa village, Lesvos, Greece where a Mw 6.3 earthquake occurred on June 12th, 2017. A dense point cloud from some digital images created based on Structure from Motion algorithm and compared with a dense point cloud acquired by a laser scanner. The distance measurement and the comparison were conducted with the Multiscale Model to Model Cloud Comparison method. According to the results, the mean of the absolute distances between the two clouds is 0.038m while the 94.9% of the point distances are less than 0.1m. Terrestrial photogrammetry proved to be an accurate methodology for rapid earthquake damage assessment thus its products were used by local authorities for the calculation of the compensation for the property loss.

1. INTRODUCTION

1.1 Introduction and literature review

The sudden hit, by with little or no warning, of an earthquake has major effect to human life and property. After an earthquake, a rapid damage assessment is vital for emergency response actions, rescue operations and post-disaster reconstructions (Tu et al. 2016). Building damage is one of the major issues that civil protection agencies should cope within crisis management of an earthquake. Various types of remote sensing data (aerial or satellite images, SAR, LiDAR) and different techniques are utilized in building damage detection and assessment, that either evaluate the changes using data before and after a disaster or interpret only data after a disaster for initial building damage evaluation and rapid response (Tu et al., 2016; Rastiveis et al., 2015; Dong and Shang, 2013). Tong et al. (2012) detected both individual collapsed building and region of buildings based on building height change using - IKONOS stereo image pairs before and after the Wenchuan earthquake. Gerke and Kerle (2011) developed a building damaged classifier based on airborne oblique, multi-perspective pictometry data. The application of oblique images assessed except from roof and facade building information that would not be visible from traditional image-based methods. Aerial imagery, UAVs and LiDAR system appeared as alternative sources of building damage information in earthquake-damaged areas (Vetrivel et al., 2015; Yamazaki et al., 2015; Galarreta et al., 2015).

Nowadays, 3D modeling is becoming very popular in documenting building environment. The texturized

photorealistic 3D models can exceptional describe the shape and size of an object with all details and high level of features accuracy. These models were widely acquired with three different survey methods: (i) photogrammetry; (ii) Terrestrial Laser Scanning (TLS); (iii) or both techniques (Lerma et al., 2010).

Aerial and terrestrial photogrammetry (TP) ranks among the methods that can be used to survey building structures and assess 3D models. This approach became more popular when photogrammetry algorithms enhanced by computer vision techniques leading to the well-known methodology of Structure from Motion (SfM) (Snavey et al., 2008). On the other hand, TLS methods have been widely used in cultural heritage and archaeology documentation through the extraction of 3D information (Rüther et al., 2012).

Many researches propose to combine and integrate both TLS and photogrammetric methods as they are capable of collecting precise and dense 3D point clouds (Lerma et al., 2010; Moussa et al., 2013; Xu et al., 2014). Li et al. (2008) proposed a 3D model and high resolution imagery fusion for reconstructing 3D building models. LiDAR data, before and after an earthquake, were also proposed for detecting building changes by measuring the rate of destroyed rooftops of building models. Galarreta et al. (2015) demonstrated that the combination of 3D point clouds with damage features extracted from oblique images can be useful for intermediate damage assessment at building level. Yamatzaki et al. (2015) highlighted the usefulness of SfM technique to depict damage situation of buildings due to 2011 Tohoku earthquake. Following the 24 August 2014 Napa earthquake, Morelan et al. (2015) used SfM to produce

* Corresponding author

extremely high-resolution 3D point clouds with an mm-scale resolution of surface rupture through anthropogenic features. Nowadays, research interest focuses on the comparison of the 3D accuracy between measurements of high resolution TLS and TP, so as to examine point cloud characteristics for accuracy assessment and suitability for different 3D applications (Nuttens et al., 2011; Widyaningrum and Gorte, 2017).

This paper aims to compare the point clouds generated from TLS and TP and evaluate whether TP based on a handheld DSLR camera can be used to map building damages, structure deformation and facade production in an acceptable accuracy. Especially, for a rapid building damage assessment after a natural disaster, a generation of a 3D model can be a useful tool for civil protection in order to assess either building damage distribution, measuring damaged surfaces and volumes, or compensation's calculations for property loss.

1.2 Study area

On 12 June 2017 a Mw 6.3 earthquake occurred offshore Lesvos Island in SE Aegean Sea, Greece (Kiratzi, 2018). Heaviest damage was reported in the village of Vrisa, where the majority of buildings constructed by stone masonry (Lekkas et al., 2017). According to the official nomenclature, engineers inspected all the 788 buildings. Nearly, 35% of the buildings suffered from very heavy damages or destruction and they characterized as beyond repair, about 39% are reported as moderate to heavy non-structural damage buildings, while 26% are characterized as buildings with negligible to slight damage.

For this research, the Vrisa village was divided into sectors, and each sector included several road sections. TP and TLS data were acquired for the entire settlement immediately after the earthquake. All surveys were conducted under real conditions with extended debris and decrepit buildings (Figure 1 - upper left and right). The weather conditions were quite extreme in some cases. For the month following the earthquake and during the working hours, the maximum air temperature was 39° and the maximum wind speed was 27.5 m/sec. In this research, we selected a road section including four buildings. Two of them were damaged beyond repair, one was damaged and needs restoration and one was undamaged (Figure 1 - down left and right).



Figure 1. Street conditions during surveys (up) and two damaged beyond repair buildings of the study area (down).

2. METHODOLOGY

2.1 Terrestrial photogrammetry

All images were acquired by two NIKON D3400 using an 18–55 mm and an 18–105 mm lens respectively. This 24.2-megapixel DSLR camera is equipped with a 23.5 mm x 15.6 mm CMOS sensor. The acquisitions performed with 18mm focal length, therefore, the dimension of each pixel of the 6000 x 4000 pixel image was 4 x 4 μm . All images were shot in “aperture priority” mode equal with f/8. It should be noticed that the vibration reduction was set to “off” because settings that aim to reduce the vibrations and stabilize the images can reduce the potential accuracy (Rieke-Zapp and Peipe, 2006). A total of 189 images were shot for this roadside section. The approximate distance between the stations and the facades were 4 m which was also the width of the road. Images were shot perpendicular to facades and at an angle of approximately 45° degrees to the X and Z axes. A hand-held mounting pole also was used to shoot photos from higher stations (Figure 2).

The quite popular Structure from Motion (SfM) and multiview stereo (MVS) approach applied for the generation of the 3D point cloud of our study area. This approach has been extensively implemented the last decade in 3D mapping in different scales. For example, Westoby et al. (2012) used terrestrial images for 3D modeling meso and micro-scale landforms while Gallo et al. (2014) applied SfM for the 3D reconstruction on objects with a bounding box diagonal ranging from 13.5 mm to 41 mm. The combination of SfM and MVS has been employed in some commercial and free software packages in different variations (Snavey et al., 2006; Wu et al., 2011). In the present study, we used the Agisoft Photoscan (Agisoft, 2018).



Figure 2. Projection centers at street level (blue) and by using mounting pole (pink).

The first step of the SfM approach is the identification of common points between the images and the generation of a descriptor for each of these points. This task is implemented through the Scale Invariant Feature Transform (SIFT) (Lowe, 1999). The user also has the ability to specify a set of points to aid the image matching, create scale bars, and check the accuracy of the procedure. In order to scale the model to the ground units, we used two artificial scale objects with known distances (Figure 3). A 2-sided wooden bar with sides 21 cm and 51 cm respectively and a 2x2 chessboard sized 18x18 cm. In the present road section, only the first scale object was identified and used. SIFT-based algorithms require images that meet specific qualitative standards for the appropriate distinction of textures appearing in the images (Wu et al., 2013). Therefore, quality control of the images applied, assuring that no blurred images will be included in the process because a tripod was not used. Furthermore, moving and other undesirable objects (i.e. sky, humans, moving trees by the wind, reflections to windowpanes, shadowed or sun glinted areas) were masked. Another problem that was met during the survey,

was the homogeneous surfaces i.e. walls and railings, and due to the available small distance between stations and objects, SIFT algorithm quite often was unable to match adjacent images. The output of the SIFT, was the list of the common points forming a sparse point cloud. These points were also used for the estimation of the camera intrinsic and extrinsic orientation parameters based on a bundle-adjustment algorithm (Triggs et al., 1999).



Figure 3. Scale objects i.e. objects with known dimensions.

Camera locations and the sparse point cloud generated from SIFT algorithm, were used to generate the final dense point cloud. Due to available processing power, the large dataset and the limited time, original images were downsampled to 25%.

2.2 Terrestrial laser scanning

Laser Scanners are active imaging instruments that use the transmission of a laser beam to calculate real-time the three-dimensional coordinates of the object being scanned. The raw data of the laser scanning process is a point cloud with x, y, z coordinates referenced to the scan reference system and i-value, the intensity of the reflected signal. Laser scanner data are one of the best data sources to quickly distinguish damaged buildings from undamaged buildings (Rastiveis et al., 2015).

The laser scanning process in the study area presented in this paper was performed using the terrestrial laser scanner Focus^{3D}, manufactured by FARO. This scanner features a full 360° x 305° field-of-view, with high scan speed (976k pts/sec) and the distance measurement is realized by the phase-shift measurement principle. On the phase-shift principle, the distance can be calculated because the phase shift between the emitted and the received laser beam at a particular wavelength is predetermined (Vosselman and Maas, 2010).

The first step was to determine the positions and the appropriate parameters setup of the scanner. The fundamental element to be taken into consideration for the positioning of the scanner is to fully cover the desired three-dimensional area, so the chosen positions should be well distributed. A single scan was not sufficient, due to occlusions and possible danger of the physical safety of the team members (near ready-to-collapse walls), thus three positions were chosen (Figure 4). Three partial scans with 120° x 305° field-of-view were captured using the Focus^{3D} laser scanner. The selected resolution was at ¼, translated at a spatial resolution (point distance) of 6.13 mm/10m and the selected quality was 2x, meaning that every point was fired two times by a laser beam for more accurate distance-value. During data collection, digital photos were captured by the integrated digital camera of the scanner. Also, measurements were taken from the

two integrated sensors of the scanner, the digital compass and inclinometer, which is useful information for the later registration of the scans.

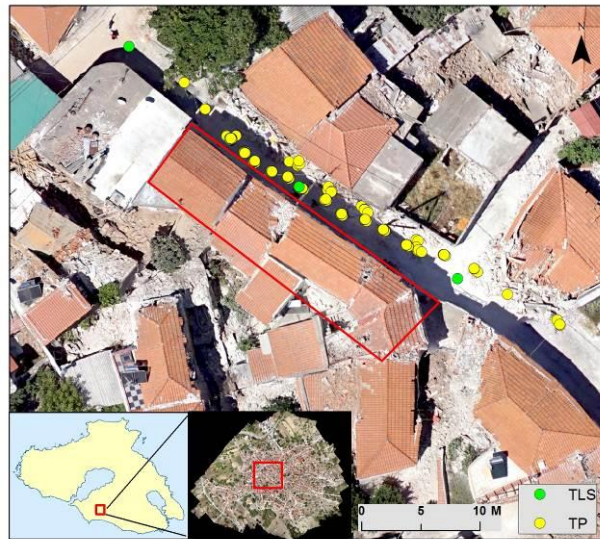


Figure 4. The study, the TLS positions and the the TP projection centers.

The acquired raw data of the laser scanner consist of individual point clouds, where their position and orientation should be changed so that each point cloud uses a universal coordinate system. This process is characterized as cloud alignment or registration, where the point clouds resulting from the different scans of the object are joined together by means of common points. Iterative Closest Point (ICP) (Besl and McKay, 1992) is the most common used algorithm for the registration of the point clouds. ICP is an iterative algorithm that affects two point clouds, and reduces the 3D alignment error at each step, gradually improving the transformation approach. It converges to the lowest local minimum of an error function, and its function is based on point matches between the two point clouds. In particular, in each iteration, the algorithm seeks to reduce the distances between the respective points, thus bringing point clouds more close. (Deng, 2011).

The registration process is differentiated according to the software, but generally uses three methods (Vosselman and Maas, 2010). The first method is called target-to-target registration and performs the clouds' alignment with the help of commonly-labeled artificial targets (such as spheres or planar checkerboards) that have been captured at each scan or physical feature-specific points visible in two consecutive scans. The second method is called cloud-to-cloud registration and attempts to align scans based on common areas, with the constraint that there is enough overlap (>30%) between two consecutive scans. The latest method is surface-to-surface registration, where the alignment of the scans is based on the geometry of its surfaces.

During the survey presented in this paper, artificial targets were not used, because it is time and effort consuming and not suitable for a post-earthquake rapid response. SCENE software by FARO (FARO, 2018) was used for the process of the scans, and the registration process took place using the cloud-to-cloud method. It is an automated registration approach which uses distinctive features extracted from point clouds, and these features have to be matched between pairwise scans in order to estimate an initial approximation for the six-parameter rigid-

body transformation, followed by an error minimization step using a surface matching algorithm like ICP.

Two filters were applied to the registered point cloud: a) an outlier removal filter to eliminate isolated and undesired points such as noise and b) the point cloud was cropped to the study area. The next step was to apply the texture on the segmented point cloud by using the acquired photos from the scanner which were automatically mapped to the corresponding point measurements. The final step was the quality assurance of the point cloud. This was done by comparing a number of control distances that were taken on fixed objects like windows and doors with the corresponding measurements on the point cloud, resulting to a deviation of less than 2mm.

2.3 Data Comparison

Comparison between two point clouds requires that both datasets must be co-registered. Observation stations of the laser scanner were georeferenced to the Greek Geodetic Reference System (GGRS87-EPSG: 2100) with the use of Real Time Kinematics (RTK) measurements. Georeferencing of all cameras' stations was not feasible because more than 20,000 images were acquired for the whole study area. Furthermore, a set of ground control points was not used due to the rapid deployment of the survey immediately after the earthquake. Finally, georeferencing to GGRS87 was accomplished by identifying common points between the images and an orthomosaic that was created during a UAV survey that took place at the same time.

For the present study a fine registration of the two datasets was required. The main methods usually applied for this task are: a) alignment by picking an adequate number of point pairs in both point clouds; and b) the Iterative Closest Point (ICP) (Besl and McKay, 1992) which also used in TLS scanning registration. It should be noticed that ICP has been extensively used in co-registration of point clouds not only on its primary form but also with hundreds of variations (Pomerleau et al., 2013). ICP was finally chosen for this research because its robustness and the better performance especially when the two datasets have small differences and overlap in a large extent. After the co-registration, the two datasets were clipped with the same bounding box, ensuring that the comparison will take place to the same spatial extent.

Various methods have been developed for the comparison of two 3D models. In this study we used the Multiscale Model to Model Cloud Comparison (M3C2) algorithm (Lague et al., 2013). The method requires that both of the 3D models are in raw point cloud format oppose to the methods that require meshes or grids. Furthermore, M3C2 is proposed for high accuracy distance measurements while other methods i.e. Cloud to Cloud (C2C) are applied for rapid change detection on very dense point clouds (Girardeau-Montaut et al., 2005). M3C2 computation is based on local normal direction rather than only on the vertical direction between points. The user defines a radius based on objects roughness and the algorithm creates a cylinder oriented along the normal vector. The intersection between the cylinder and the points clouds, defines two point subsets for which the mean distance is computed. Usually, the user defines a point cloud as a reference, however we would like to examine the areas that can be seen by TLS and not from TP and vice versa. Thus, we estimated both distances by assigning as a reference point cloud, the point clouds from both methodologies. Both ICP and M3C2 algorithm applied through

the open source software CloudCompare (Girardeau-Montaut, 2018). The overall workflow of this research is shown in Figure 5.

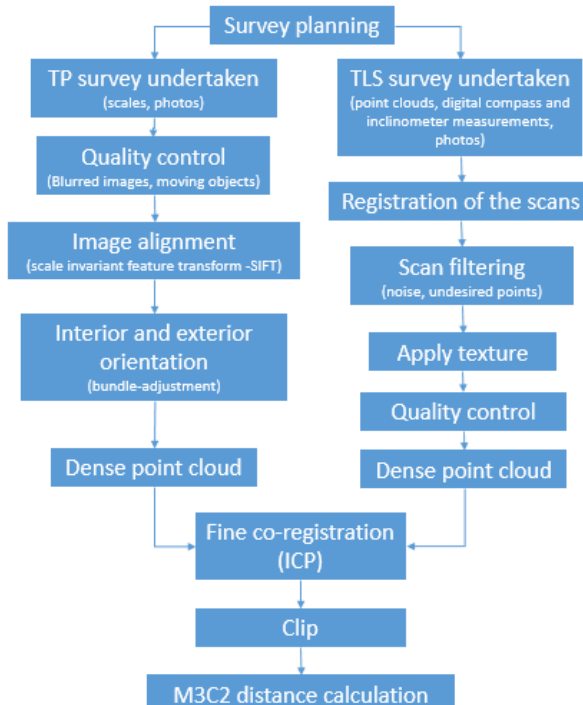


Figure 5. Workflow of the applied methodology.

3. RESULTS AND DISCUSSION

3.1 Point clouds generation

The alignment of the 189 images required 48,409 tie points that were automatically identified by the SIFT algorithm. Thirteen checkpoints were required in order to assist the alignment. The reprojection error was 1.81 pixel and the final ground resolution of the images given the distance between the camera stations and the houses was 0.763 mm/pixel. Finally, 3 control points were used for the georeferencing resulting in Root Mean Square (RMS) error 7.57 cm while the error at the scale bars was 1.02 cm. The area covered by the facades of the four houses of this road section was 130 m².

Regarding TLS methodology, the mean registration error of the three scans was 2.3715 mm. A percentage of 66.3% (Figure 6) and 66.7% (Figure 7) had an error less than 4 mm on pairwise registered point clouds. That error represents the distance where a specific point has been calculated between two consecutive scans. The point density of the registered point cloud was very high (41M points) due to the massive overlap of the consecutive scans pairwise (53.4% and 40.9%).

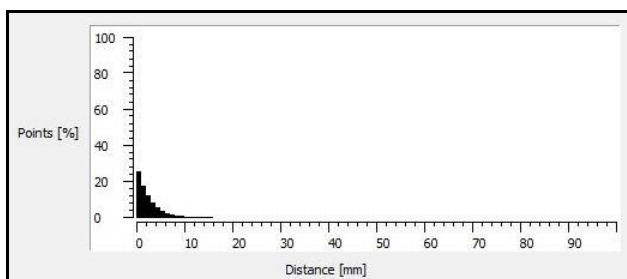


Figure 6. Registration Distance Histogram
(scanner positions 1-2).

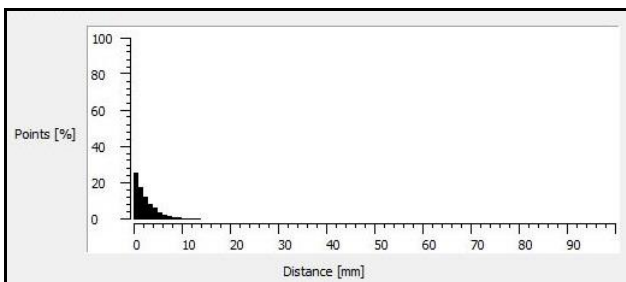


Figure 7. Registration Distance Histogram
 (scanner positions 2-3)

Next step was the fine co-registration of both datasets with the ICP algorithm. Registration was based on 50,000 random sampling points and the process would stop either if the computation would exceed the 20 iterations or the RMS error would drop more than 10^{-5} between two consecutive iterations. The theoretical overlap between the two datasets was set to 90%. The RMS error from this procedure was 3.58 cm. Figure 8 shows the final point clouds of the 2 methodologies cropped to the same extent. It can be seen that both methodologies capture the facades in a similar way. Blind spots are created a) at the second floor due to balconies; and b) at doors or windows that are installed in a niche (Figure 9). These spots are quite often at TLS approach due to fewer scanning positions (Figure 4).



Figure 8. Cloud point based on terrestrial photogrammetry (up) and laser scanning (down).

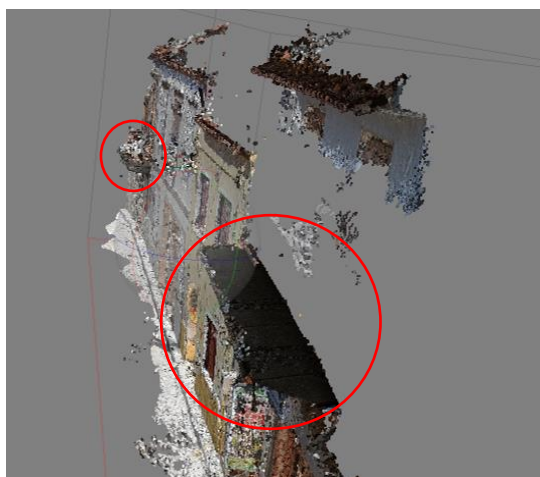


Figure 9. Facade extensions (i.e. balconies) creating blind spots.

Concerning the point density of the generated clouds, TLS produced locally a higher density point cloud with higher mean value equal to 142,458 points per 0.0314 m^2 . However, the density of the TP point clouds is uniform throughout the facades with a mean value of 121,399 points per 0.314 m^2 . On the other hand, TLS present the higher density at the center of the scene (Figure 10). The nature of TLS approach resulted to the convergence of the sight beams to the center of the study area and the irregular distribution of the point density.

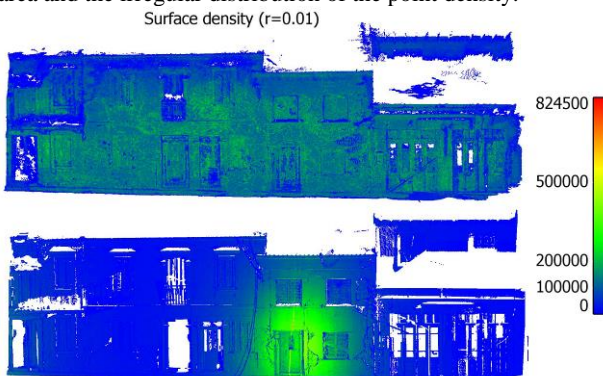


Figure 10. Cloud point density based on terrestrial photogrammetry (up) and laser scanning (down).

3.2 Point cloud comparison

The M3C2 algorithm execution reveals that the point clouds produced by the two methodologies can similarly describe the facades and the roughness of the buildings (Figure 11). When using the TLS point cloud as a reference, the mean absolute difference is 3.8 cm while the 94.9% of the computed differences are lower than 10 cm (Figure 12). The higher differences are observed at the right side of the study area even though differences are still less than 10cm. This is due to the fact that fewer camera stations locate at this area. (Figure 4). The 5% of points that are in distance greater than 10 cm are detected mainly in two areas. At the left side of the study area the damaged door of a building exposes the inner house which can be scanned by the TLS approach but cannot be photographed because of the light conditions. Another subset of points that seems to be misplaced between the 2 point clouds is an area that is behind glass windows. Optical properties of materials such as glass windows is a common error source of TLS and the distance measurement is affected and limited by the physical laws of reflection, including refraction and inner reflection effects (Ingensand et al., 2003). Thus, the surface reflection on glass of a laser beam normally causes reflected beams in many directions.



Figure 11. Absolute difference between TP and TLS point clouds setting the TLS dataset as reference (up) and TP dataset as reference (down)

When using the TP point cloud as a reference, results are quite similar. The mean absolute difference is 5.6 cm while the 91.4% of the computed differences are lower than 10 cm. By using as referencing both point clouds during distance estimation, we see that the 94.9% of the point cloud generated by TP overlaps the point cloud of TLS within a distance of 10 cm while the 86.9% of the TLS point cloud overlaps the dataset from TP within the same distance.

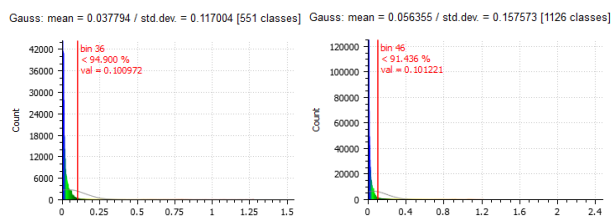


Figure 12. Histograms of the absolute differences between TP and TLS point clouds setting the TLS dataset as reference (left) and TP dataset as reference (right)

4. CONCLUSIONS

3D mapping of damaged buildings can provide significant data towards developing a building information model. These data can be used as inputs to various methodologies for estimating costs and failures. Two of the most popular methods for 3D data generation are the terrestrial photogrammetry based on DSLR images and the terrestrial laser scanning. Within this research we evaluated whether terrestrial photogrammetry is a reliable methodology to create a 3D model with acceptable accuracy. Comparing to laser scanners, terrestrial photogrammetry is based on low-cost equipment such as DSLR cameras and smartphones. The SfM processing approach and the software supporting it, are more user-friendly to non-expert users although a basic background of analytic photogrammetry is critical for survey planning and results in evaluation. The exploitation of the 3D output models from the above processing was succeeded as embedded 3D objects in pdf files. The civil protection agencies of Greece used these models for a complete representation of the post-physical state of the Vrisa's buildings. Based on the measurements that can be retrieved from the 3D model within the pdf file, agencies calculated the compensation for the property loss. Furthermore, the extracted models are valuable components that help engineering to understand the seismic behaviour in a more comprehensible way.

ACKNOWLEDGEMENTS

This paper is a result of the research project “3D mapping of Vrisa settlement after the 12th June Lesvos earthquake” funded by the North Aegean Region.

REFERENCES

Agisoft, 2018. Agisoft PhotoScan User Manual, Professional Edition, Version 1.2, http://www.agisoft.com/pdf/photoscan-pro_1_2_en.pdf (7 February 2018).

Besl, P. J. and McKay, N. D., 1992. A method for registration of 3-D shapes. *IEEE Transactions on Pattern Analysis and Machine Intelligence*, 14(2), pp. 239-256. <https://doi.org/10.1109/34.121791>

Deng, F., 2011. *Laser Scanning, Theory and Applications*. (C.C. Wang, Ed.), InTech, Rijeka, Croatia, pp. 449-472. <https://doi.org/10.5772/630>

Dong, L. and Shan, J., 2013. A comprehensive review of Earthquake-induced building damage detection with remote sensing techniques. *ISPRS Journal of Photogrammetry and Remote Sensing*, 84, pp. 85-99 <https://doi.org/10.1016/j.isprsjprs.2013.06.011>

FARO, 2018. FARO SCENE: FARO’s 3D Documentation Software for terrestrial and handheld Scanners, Version 7.0, <https://www.faro.com/products/product-design/faro-scene/> (7 February 2018).

Galarreta, J.F., Kerle, N., and Gerke, M., 2015. UAV-based urban structural damage assessment using object-based image analysis and semantic reasoning. *Natural Hazards Earth Systems Sciences*, 15, pp. 1087-1101 <https://doi.org/10.5194/nhess-15-1087-2015>

Gallo, A., Muzzupappa, M., and Bruno, F., 2014. 3D reconstruction of small sized objects from a sequence of multi-focused images. *Journal of Cultural Heritage*, 15(2), pp. 173-182 <https://doi.org/10.1016/j.culher.2013.04.009>

Gerke, M. and Kerle, N., 2011. Automatic structural seismic damage assessment with airborne oblique pictometry imagery. *Photogrammetric Engineering and Remote Sensing*, 77(9), pp. 885-898.

Girardeau-Montaut, D., Roux, M., Marc, R., and Thibault, G., 2005. Change detection on points cloud data acquired with a ground laser scanner. *ISPRS - International Archives of the Photogrammetry, Remote Sensing and Spatial Information Sciences*, 36(3), pp. 30-35.

Girardeau-Montaut, D., 2018. CloudCompare 3D point cloud and mesh processing software, Version 2.6.3, <http://www.danielgm.net/cc/> (7 February 2018).

Ingensand, H., Ryf, A. and Schulz, T., 2003. Performances and Experiences in Terrestrial Laserscanning. In: *Proceedings of the 6th Conference on Optical 3D Measurement Techniques*, Zurich.

Kiratzi, A., 2018. The 12 June 2017 Mw 6.3 Lesvos Island (Aegean Sea) earthquake: Slip model and directivity estimated with finite-fault inversion. *Tectonophysics*, 724-725, pp. 1-10 <https://doi.org/10.1016/j.tecto.2018.01.003>

Lague, D., Brodu, N., and Leroux, J., 2013. Accurate 3D comparison of complex topography with terrestrial laser scanner: Application to the Rangitikei canyon (N-Z). *ISPRS Journal of Photogrammetry and Remote Sensing*, 82, pp. 10-26 <https://doi.org/10.1016/j.isprsjprs.2013.04.009>

Lekkas, E., Mavroulis, S., Skourtos, E., Andreadakis, E., Antoniou, V., Kranis, C., Soukis, K., Lozios, S., and Alexoudi, V., 2017. Earthquake environmental effects induced by the 2017 June 12, Mw 6.3 Lesvos (North Aegean Sea, Greece) earthquake. In: *8th International INQUA Meeting on Paleoseismology, Active Tectonics and Archeoseismology (PATA)*, 13-16 November, 2017, New Zealand.

- Lerma, J.L., Navarro, S., Cabrelles, M., and Villaverde, V., 2010. Terrestrial laser scanning and close range photogrammetry for 3D archaeological documentation: the Upper Palaeolithic Cave of Parpalló as a case study. *Journal of Archaeological Science*, 37(3), pp. 499-507 <https://doi.org/10.1016/j.jas.2009.10.011>
- Li M., Cheng L., Gong J., Liu Y., Chen Z., Li F., Chen G. and Song X. (2008). Post-earthquake assessment of building damage degree using LiDAR data and imagery. *Science in China Series E: Technological Sciences*, Vol 51. 133-143pp. <https://doi.org/10.1007/s11431-008-6014-1>
- Lowe, D.G., 1999. Object recognition from local scale-invariant features. In: *The Proceedings of the Seventh IEEE International Conference on Computer Vision*, pp. 1150-1157 <https://doi.org/10.1109/ICCV.1999.790410>
- Morelan, A.E., Trexler C.C., and Oskin, M.E., 2015. Rapid documentation of earthquake surface displacements using structure from motion photogrammetry. *American Geophysical Union Fall Meeting*, abs. T31A-2840.
- Moussa, W., Wenzel, K., Rothermel, M., Abdel-Wahab, M., and Fritsch, D., 2013. Complementing TLS Point Clouds by Dense Image Matching. *International Journal of Heritage in the Digital Era*, 2(3), pp. 453-470 <https://doi.org/10.1260%2F2047-4970.2.3.453>
- Nuttens, T., De Maeyer, Ph., De Wulf, A., Goossens, R., and Stal, C., 2011. Terrestrial Laser Scanning and Digital photogrammetry for Cultural Heritage: an Accuracy Assessment. FIG Working Week 2011, Marrakech, Morocco, 18-22 May 2011.
- Pomerleau, F., Colas, F., Siegwart, R., and Magnenat, S., 2013. Comparing ICP variants on real-world data sets. *Autonomous Robots*, 34(3), pp. 133-148.
- Rastiveis, H.; Eslamizade, F.; Hosseini-Zirdoo, E. (2015): Building damage assessment after earthquake using post-event LiDAR data. *ISPRS - International Archives of the Photogrammetry, Remote Sensing and Spatial Information Sciences*, XL-1-W5, pp. 595-600 <https://doi.org/10.5194/isprarchives-XL-1-W5-595-2015>
- Rieke-Zapp, D.H. and Peipe, J., 2006. Performance evaluation of a 33 megapixel alpa 12 medium format camera for digital close range photogrammetry. In: *The International Archives of the Photogrammetry, Remote Sensing and Spatial Information Sciences*, XXXVI(5).
- Rüther, H., Bhurtha, R., Held, C., Schröder, R., and Wessels, S., 2012. Laser Scanning in Heritage Documentation: The Scanning Pipeline and its Challenges. *Photogrammetric Engineering and Remote Sensing*, 78(4), pp. 309-316.
- Snavely, N., Seitz, S.M., and Szeliski, R., 2006. Photo tourism: exploring photo collections in 3D. *ACM Transactions on Graphics (TOG) - Proceedings of ACM SIGGRAPH 2006*, ACM., 25(3), pp. 835-846 <https://doi.org/10.1145/1141911.1141964>
- Snavely, N., Seitz, S.M., and Szeliski, R. 2008. Modeling the world from Internet photo collections. *International Journal of Computer Vision*, 80(2), pp. 189-210 <https://doi.org/10.1007/s11263-007-0107-3>
- Tong, X., Hong, Z., Liu, S., Zhang, X., Xie, H., Li, Z., Yang, S., Wang, W., and Bao, F., 2012 Building damage detection using pre- and post-seismic high resolution satellite stereo imagery: A case study of May 2008 Wenchuan earthquake. *ISPRS Journal of Photogrammetry and Remote Sensing*, 68(2), pp. 13-27 <https://doi.org/10.1016/j.isprsjprs.2011.12.004>
- Triggs, W., McLauchlan, P., Hartley, R., and Fitzgibbon, A., 1999. Bundle adjustment: A modern synthesis. In: *Vision Algorithms: Theory and Practice*, number 1883 in LNCS. Springer-Verlag. Corfu, Greece, pp. 298-373.
- Tu, J., Sui, H., Feng W., and Song, Z., 2016. Automatic Damage Detection Method Using High-Resolution Remote Sensing Images and 3D GIS Model. *ISPRS Annals of the Photogrammetry, Remote Sensing and Spatial Information Sciences*, III-8, pp. 43-50 <https://doi.org/10.5194/isprs-annals-III-8-43-2016>
- Vetrivel, A., Gerke, M., Kerle, N., and Vosselman, G., 2015. Identification of damage in buildings based on gaps in 3D point clouds from very high resolution oblique airborne images. *ISPRS Journal of Photogrammetry and Remote Sensing*, 105, pp. 61-78 <https://doi.org/10.1016/j.isprsjprs.2015.03.016>
- Vosselman, G. and Maas, H. G., 2010. *Airborne and Terrestrial Laser Scanning*. Whittles Publishing, Boca Raton, FL, USA, pp. 109-118.
- Westoby, M.J., Brasington, J., Glasser, N.F., Hambrey, M.J., and Reynolds J.M., 2012. Structure-from-motion' photogrammetry: A low-cost, effective tool for geoscience applications. *Geomorphology*, 179, pp. 300-314.
- Widyaningrum, E., and Gorte, B., 2017. Comprehensive comparison of two image-based point clouds from aerial photos with airborne lidar for large-scale mapping: Door detection to envelope reconstruction. In: *The International Archives of the Photogrammetry, Remote Sensing and Spatial Information Sciences*, XLII-2/W7, pp. 557-565 <https://doi.org/10.5194/isprarchives-XLII-2-W7-557-2017>
- Wu, C., Agarwal, S., Curless, B., and Seitz, S.M., 2011. Multicore bundle adjustment. In: *2011 IEEE Conference on Computer Vision and Pattern Recognition (CVPR)*, pp. 3057-3064 <https://doi.org/10.1109/CVPR.2011.599552>
- Wu, J., Cui, Z., Sheng, V.S., Zhao, P., Su, D., and Gong, S., 2013. A Comparative Study of SIFT and its Variants. *Measurement Science Review*, 13(3), pp. 122-131 <https://doi.org/10.2478/msr-2013-0021>
- Xu, Z., Wu, L., Shen, Y., Wang, Q., Wang, R., and Li, F., 2014. Extraction of damaged building's geometric features from multi-source point clouds. In: *2014 IEEE International Geoscience and Remote Sensing Symposium (IGARSS)*, pp. 4764-4768 <https://doi.org/10.1109/IGARSS.2014.6947559>
- Yamazaki, F., Matsuda, S., Denda, S., and Liu, W., 2015. Construction of 3D models of building damaged by earthquakes using UAV aerial images. In: *Proceedings of the Tenth Pacific Conference on Earthquake Engineering Building an Earthquake-Resilient Pacific*, 6-8 November, Sydney, Australia.